Chemical Engineering Journal xxx (2017) xxx–xxx

Contents lists available at ScienceDirect

Chemical Engineering Journal

journal homepage: www.elsevier.com/locate/cej

Surface barriers as dominant mechanism to transport limitations in hierarchically structured catalysts – Application to the zeolite-catalyzed alkylation of benzene with ethylene

Sanjeev M. Rao [a,1], Erisa Saraçi [b,2], Roger Gläser [b], Marc-Olivier Coppens [c,*]

[a] Howard P. Isermann Department of Chemical and Biological Engineering, Rensselaer Polytechnic Institute, Troy, NY 12180, USA
[b] Institute of Chemical Technology, University of Leipzig, Linnéstraβe 3, Leipzig 04103, Germany
[c] Department of Chemical Engineering, University College London, Torrington Place, London WC1E 7JE, United Kingdom

HIGHLIGHTS

- The total meso- plus macroporosity of a hierarchical zeolite must be optimized.
- The reaction yield for benzene ethylation is doubled over a pure zeolite pellet.
- Modeling results are compared with fixed bed reactor experiments.
- Surface barriers might limit the performance of hierarchically structured zeolites.

ARTICLE INFO

Article history:
Available online xxxx

Keywords:
Surface barriers
Diffusion
Meso-macropore network
Zeolites
Rational catalyst design
Benzene alkylation

ABSTRACT

The meso-macropore network of a hierarchically structured zeolite catalyst is numerically optimized to maximize the volume-integrated reaction yield in the ethylation of benzene to produce ethylbenzene over zeolite H-ZSM-5. A hierarchical approach is used at multiple length scales to determine the optimal pore network properties. The maximum volume-integrated reaction yield of the hierarchically structured zeolite catalyst containing meso- and macropores is nearly twice the yield of a zeolite pellet containing only macropores, at the same macroporosity. To bridge the gap between modeling and experiments, a series of physical mixtures of ZSM-5 crystals and mesoporous silica, containing different weight fractions of zeolite is synthesized and used in fixed bed reactor experiments to determine the optimal pellet structure to maximize the conversion of ethylene. Comparison with reactor simulations of the zeolite composites shows that the performance of the zeolite composites might be limited by surface barriers at the external surface of the zeolite crystals, rather than by diffusion limitations within the meso-macropore network of the pellets.

1. Introduction

Rational catalyst design often focuses on the nanoscale, where it is aided by insights from both quantum chemical calculations [1] and experimental characterization methods, such as spectroscopy and electron microscopy [2,3], approaching atomic resolution, to identify the nature of the active surface species, elucidate the role of active sites in reaction mechanisms and inform intrinsic kinetics. Over the past twenty years, there has also been significant development in the availability of material synthesis techniques, which allow for increasing control over the pore structure of a catalyst at multiple length scales [4–6]. However, this microscopic design framework tends to neglect the equally important task of preserving the tailored properties of a catalyst up to macroscopic length scales, namely those of the catalyst pellet and the reactor it is used in. The latter is relevant in practical applications [7–13], where catalyst performance is often limited by diffusion limitations and catalyst deactivation. Therefore, the topic of rational catalyst design must encompass all length scales. It is crucial to identify those features of the pore network in a catalyst pellet that significantly influence catalyst performance for industrially important reactions, such as reforming and alkylation. Doing so will enable the catalyst manufacturer and the process licensor to reduce the time

* Corresponding author.
E-mail address: m.coppens@ucl.ac.uk (M.-O. Coppens).
[1] Present address: SABIC Americas, Sugar Land, TX, USA.
[2] Present address: University of Delaware, Newark, DE, USA.

http://dx.doi.org/10.1016/j.cej.2017.04.015
1385-8947/

List of symbols

$[B]$	matrix of Maxwell Stefan mobilities and loadings
$\mathcal{D}_i$	corrected diffusivity or mobility of species i in the zeolite (m^2/s)
$D_{e,i}$	effective diffusivity of species i in the mesopores ($m_f^3/m_g/s$)
$D_{E,i}$	effective diffusivity of species i in the macropores ($m_f^3/m_p/s$)
D_{ij}	binary diffusivity of species i and j ($m_f^3/m_f/s$)
D_{Ki}	Knudsen diffusivity of species i ($m_f^3/m_f/s$)
F_i	molar flowrate of species i (mol/s)
F_t	total molar flowrate (mol/s)
k_f	forward rate constant for the benzene alkylation reaction, (1/s)
k_b	reverse rate constant for the benzene alkylation reaction, (1/s)
L	length of the catalyst bed (m_r)
N_i	flux of species i ($mol/m^2/s$)
p_{is}	partial pressure of species i (Pa)
p_{is}^s	partial pressure of species i at the external surface of the zeolite, grain or pellet (Pa)
p_t	total pressure (Pa) or (bar)
q_{is}	molar loading of species in the zeolite (mol/kgcat)
q_{is}^s	molar loading of species at the external surface of the zeolite (mol/kgcat)
r	rate of reaction (mol/kgcat/s)
R	radius (m)
R_g	universal gas constant (J/mol/K)
T_s	temperature (K)
x	conversion
z	axial coordinate along the length of the fixed bed reactor (m_r)

Greek

α	surface permeability (m/s)
$[\Gamma]$	matrix of thermodynamic correction factors
ε	porosity, (m_f^3/m_g^3 or m_f^3/m_p^3)
ε_z	volume fraction of zeolite within the grain (m_{cat}^3/m_g^3)
η	effectiveness factor
λ	number of Brønsted acid sites per unit cell
ν_i	stoichiometric coefficient of species i
ξ	radial coordinate (m)
ρ	density (kg/m^3)
τ	tortuosity factor

Subscripts

0	reference or initial value
Bs	benzene within the porous catalyst
Es	ethylene within the porous catalysts
EBs	ethylbenzene within the porous catalyst
$E+B,H^+$	Co – adsorbed ethylene plus benzene on the Brønsted acid site
EB,H^+	adsorbed ethylbenzene on the Brønsted acid site
g,grain	grain level
m	mesopores
M	macropores
p,pellet	pellet level
s	porous catalyst
Si	mesoporous silica
z	zeolite

and effort required to screen catalyst formulations for a given process, maximize the performance of their catalysts, and help establish a framework for the rational design of hierarchically structured porous catalysts at all length scales.

Coppens and co-workers have carried out extensive studies centered on the optimization of the micro/meso-macropore network of hierarchically structured catalysts, via mathematical and computational modeling, to reduce diffusion limitations [14,15] and mitigate the effects of catalyst deactivation by site poisoning and pore blockage [16,17]. They were able to show that introducing an optimized broad pore network characterized by uniform macroporosity and constant, optimal macropore size could significantly improve the volumetric reaction yield and increase the robustness towards catalyst deactivation, when compared with a purely micro/mesoporous (nanoporous) catalyst. As long as the porosity is sufficiently connected, they also demonstrated that introducing an optimized spatial and size distribution of macroporosity and macropore diameters did not lead to significant improvements over an optimized uniform macropore network, which is an important result from the standpoint of catalyst preparation. Keil and co-workers [18–21] employed both continuum and discrete pore network models to optimize the performance of hierarchically structured porous catalysts for industrially important reactions. While these studies have examined the optimization of hierarchically structured nano-macroporous catalysts, there has been no concerted effort to combine mathematical modeling and optimization studies with experiments. Secondly, given the vast body of literature focused on the synthesis of hierarchically structured zeolites [22–26], there is presently no work that provides guidance on the nature of the optimal pore structures for a given process, so that subsequent synthesis efforts can focus on producing the desired catalyst. Hence, there is a gap between materials chemistry and engineering in hierarchical catalyst design. As a step towards achieving the goal of rational catalyst design at all length scales, this work describes the numerical optimization of a hierarchically structured zeolite pellet to maximize the production of ethylbenzene in the ethylation of benzene over the acidic medium-pore zeolite H-ZSM-5 (a reaction chosen for reasons discussed further on), and compares the activity of different meso/macroporous zeolite composites in fixed bed reactor experiments with the numerically predicted performance of these catalyst pellets.

In addition, the topic of surface barriers in zeolite catalysis and their role in overall diffusion properties has also received increased attention, in part due to the availability of sophisticated characterization tools, such as interference and infrared microscopy [27,28] that allow for distinguishing the molecular uptake rates between different zeolite crystals synthesized in the same batch. Kärger and co-workers [29] have recently demonstrated that methanol uptake in single SAPO-34 crystals differs from one crystal to the other due to varying surface permeabilities; however, the uptake rates integrated over a large number of crystals in a batch can lead to the conclusion that intracrystalline diffusion rather than the surface barrier is rate limiting. Dauenhauer and co-workers [30,31] have also extensively investigated the importance of surface barriers for zeolite crystals using zero-length chromatography (ZLC), and have proposed that the adsorption of molecules from the gas phase on to the external surface of the zeolite crystal is characterized by a different rate constant than the rate of desorption of molecules from the external surface. Keil and co-workers [32–34]

Please cite this article in press as: S.M. Rao et al., Surface barriers as dominant mechanism to transport limitations in hierarchically structured catalysts – Application to the zeolite-catalyzed alkylation of benzene with ethylene, Chem. Eng. J. (2017), http://dx.doi.org/10.1016/j.cej.2017.04.015

have carried out extensive molecular simulations of diffusion in zeolites, accounting for surface barriers in both ideal and non-ideal structures. They note that, in ideal crystal structures, surface barriers arise out of purely entropic effects, whereas, in non-ideal structures, crystal defects and pore blockage are responsible for the surface barriers. Lercher and co-workers [35–37] used time-resolved infrared spectroscopy and frequency-response measurements to demonstrate that post-synthetic modification of the external surface of ZSM-5 crystals with silica makes it easier for molecules to traverse the surface barrier, resulting in increased rates of diffusion of aromatics, such as benzene and toluene. In light of these studies, for the first time, surface barriers are also accounted for in the present study in the mathematical description of diffusion and reaction within zeolite composite pellets, in order to understand the impact of surface barriers on the performance of hierarchically structured zeolites.

The alkylation of benzene with ethylene over the zeolite H-ZSM-5 is an industrially important reaction, because ethylbenzene is an intermediate in the production of styrene. Hansen et al. [38] have determined the intrinsic kinetics of the benzene ethylation reaction using a combination of quantum chemical calculations and microkinetic modeling. In addition, they also calculated the adsorption isotherms and diffusion coefficients within a zeolite crystal for the species in the reaction system. Li et al. [39] recently used this model to simulate the behavior of an industrial zeolite pellet and determined that a random distribution of zeolite crystals within the pellet was optimal, when compared with an imposed spatial distribution of zeolite crystals within the pellet.

In this work, mathematical models were derived to simulate diffusion and reaction at three scales: (1) a zeolite crystal; (2) a "grain" composed of silica nanoparticles and zeolite crystals, with mesopores in between, and (3) a catalyst pellet composed of grains, with macropores in between. Diffusion within the zeolite crystals was first explicitly accounted for in order to determine a zeolite-level effectiveness factor. The effect of surface barriers was not included in this calculation. Next, the zeolite crystal model was coupled to a grain model in order to calculate an effectiveness factor at the grain level, as well as a volume integrated reaction yield. The weight fraction of the zeolite was varied to find the maximum volume-integrated reaction yield for which the effectiveness factor of the grain was greater than 95%. The lower bound on the grain-level effectiveness factor ensures that there are no internal diffusion limitations within the grain. This optimized grain structure was then incorporated into single-pellet simulations wherein the macroporosity was optimized to maximize the volume-integrated reaction yield at the pellet scale. In this manner, the total meso- plus macroporosity is optimized. In this work, neither the mesopore diameter nor the macropore diameter are treated as optimization variables, but rather they are simulated using experimentally measured values from the composites. Surface barriers can be accounted for by varying the boundary condition at the external surface of the zeolite crystals in either the grain or pellet scale models. The pellet scale model is then combined with a fixed bed reactor model in order to predict the exit conversion of ethylene and benzene for different hierarchically structured zeolites, which are then compared with experimental results. It is shown, for the first time, that surface barriers might play a very significant role in determining the catalytic properties of hierarchically structured zeolites.

2. Mathematical model

Fig. 1 illustrates the hierarchical model employed to describe the catalyst pellet, as already discussed in Section 1. The following sub-sections describe the equations that constitute the mathematical model.

2.1. Diffusion and reaction within a single zeolite crystal—effectiveness factor

The alkylation of benzene with ethylene over the zeolite H-ZSM-5 is described by the following reaction:

$$C_2H_4 + C_6H_6 \leftrightarrow C_8H_{10}$$

The intrinsic kinetics for this reaction are given by Hansen et al. [38] as:

$$r = k_f q_{E+B,H^+} - k_b q_{EB,H^+} \tag{1}$$

In Eq. (1), r is the rate of the reaction, k_f is the forward rate constant and k_b is the reverse rate constant. The concentrations of the co-adsorbed ethylene and benzene, and of the adsorbed ethylbenzene on the Brønsted acid site are denoted by, respectively, q_{E+B,H^+} and q_{EB,H^+}. These concentrations, in turn, are given by the following expressions:

$$q_{E+B,H^+} = \frac{q_{Bs}}{(22 - 3.25q_{Bs} - 3.5q_{EBs})} q_{Es} \frac{q_{Bs}}{(q_{Bs} + q_{EBs})} \lambda \tag{2}$$

$$q_{EB,H^+} = q_{EBs} \frac{q_{EBs}}{(q_{Bs} + q_{EBs})} \lambda \tag{3}$$

In Eqs. (2) and (3), the variables q_{Es}, q_{Bs}, q_{EBs} represent the molar loadings in the adsorbed phase within the zeolite crystal of ethylene, benzene and ethylbenzene, respectively. The acid site density of the zeolite crystal is accounted for through the number of acid sites per intersection in each unit cell, and denoted by the variable λ in Eqs. (2) and (3). Diffusion and reaction within the zeolite crystal is modeled assuming a spherical geometry and using the Maxwell-Stefan equations describing multicomponent diffusion, and the Ideal Adsorbed Solution Theory (IAST) [38]:

$$\frac{1}{\xi_z^2} \frac{d}{d\xi_z} (\xi_z^2 N_i) = \nu_i r(q_{Es}, q_{Bs}, q_{EBs}) \tag{4}$$

In Eq. (4), ξ_z is the radial coordinate in the zeolite crystal, N_i is the flux of species i and ν_i is the stoichiometric coefficient of species i. The flux vector is obtained as:

$$(N) = -\rho_z [B]^{-1} [\Gamma] \nabla (q) \tag{5}$$

In Eq. (5), ρ_z is the density of the zeolite crystal, $[B]$ is the matrix of Maxwell-Stefan diffusion coefficients, $[\Gamma]$ is the matrix of thermodynamic correction factors and (q) is the vector of molar loadings within the zeolite. The boundary conditions needed to solve equation (4) are:

$$p_{is} = p_{is}^s \text{ at } \xi_z = R_z \tag{6a}$$

$$\frac{dp_{is}}{d\xi_z} = 0 \text{ at } \xi_z = 0 \tag{6b}$$

In Eq. (6a), p_{is}^s is the partial pressure at the external surface of the zeolite crystal of radius R_z. If surface barriers are important, then the use of a Dirichlet boundary condition, as shown in Eq. (6a), is not accurate, and, instead, a Neumann boundary condition of the form shown below in Eq. (6c) should be employed:

$$\left(Đ_i \frac{dq_{is}}{d\xi} \right)_{\xi = R_z} = \alpha [f(p_{is}) - q_{is}^s] \tag{6c}$$

In Eq. (6c), $Đ_i$ is the intracrystalline diffusivity of species i in the zeolite, and α is the surface permeability of the external surface of the zeolite crystals, which quantifies the surface barrier effect. The surface permeability is assumed to be equal for all species in this

Please cite this article in press as: S.M. Rao et al., Surface barriers as dominant mechanism to transport limitations in hierarchically structured catalysts – Application to the zeolite-catalyzed alkylation of benzene with ethylene, Chem. Eng. J. (2017), http://dx.doi.org/10.1016/j.cej.2017.04.015

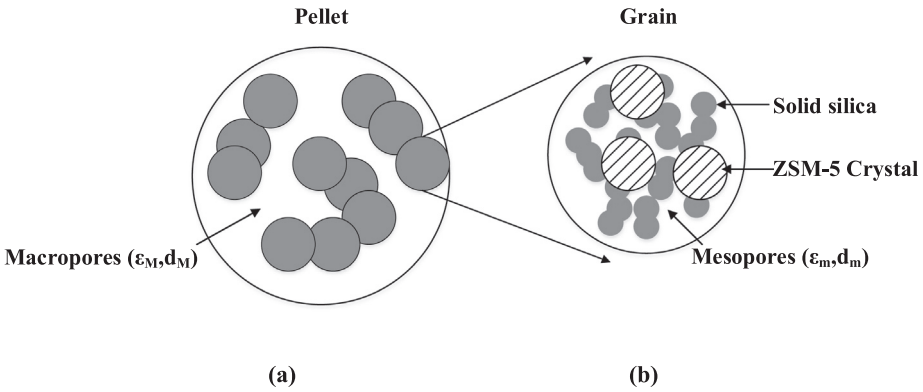

Fig. 1. Geometric representation of a catalyst pellet, comprising of agglomerates of overlapping grains separated by macropores. The grains, in turn, consist of ZSM-5 crystals embedded in a mesoporous silica matrix. (a) Pellet (b) Grain.

system; this aspect is discussed in more detail in Section 4.4. The partial pressures of the different components, p_{is}, are used to calculate the adsorbed phase molar loadings, q^s_{is}, at the external surface of the zeolite, using the Ideal Adsorbed Solution Theory (IAST) of Myers and Prausnitz [40]. For the case where surface barriers are important, the IAST is used to calculate the adsorbed phase molar loadings in equilibrium with the bulk phase partial pressure, and then substituted in Eq. (6c). The solution of the diffusion-reaction equation (4) is used to calculate the effectiveness factor at the level of the zeolite crystals as:

$$\eta_z = \frac{3}{R_z^3}\frac{\int_0^{R_z} r(p_{Es}, p_{Bs}, p_{EBs})\xi_z^2 d\xi_z}{r(p^s_{Es}, p^s_{Bs}, p^s_{EBs})} \tag{7}$$

Thus, Eq. (7) can be used to determine a zeolite crystal size for which the effectiveness factor of the zeolite is >95%. The reason for this calculation is that previous work [14–17] has shown that, in the optimal hierarchical structures, there are no internal diffusion limitations within the nanoporous (micro- or mesoporous) catalytic regions.

2.2. Diffusion and reaction within a single mesoporous grain, containing zeolite crystals and silica nanoparticles

At the scale of an isothermal composite grain, the equation for diffusion and reaction of each component is written as:

$$\frac{1}{\xi_g^2}\frac{d}{d\xi_g}\left(\xi_g^2 \frac{D_{e,i}}{R_g T_s}\frac{dp_{is}}{d\xi_g}\right) = \nu_i \eta_z r(p_{Es}, p_{Bs}, p_{EBs})\rho_g \tag{8}$$

In Eq. (8), ξ_g is the radial coordinate along the grain radius, $D_{e,i}$ is the effective diffusivity of species i in the mesopores, R_g is the gas constant, T_s is the temperature at the external surface of the grain, p_{is} is the partial pressure profile within the grain, η_z is the effectiveness factor of the zeolite crystal and ρ_g is the density of the composite grain consisting of zeolite crystals and silica. The effective diffusivity of each component is calculated using Bosanquet's formula, and correcting for the porosity and the tortuosity factor of the mesopores [41]:

$$D_{e,i} = \frac{\varepsilon_{sm}}{\tau_{sm}}\left(\frac{D_{Ki}D_{ij}}{D_{Ki} + D_{ij}}\right) \tag{9}$$

The use of the Bosanquet approximation is justified because benzene is used in molar excess in the alkylation reaction to suppress oligomerization of ethylene, and the conversion of benzene is comparatively small (around 10%). The bulk diffusivities are computed by assuming binary diffusion of ethylene and ethylbenzene through benzene. In this study, the tortuosity factor is calculated as a function of the mesoporosity, using the expression as given by Evans et al. [42]:

$$\tau_{sm} = \frac{\varepsilon_{sm}}{0.4\varepsilon_{sm} - 0.0328} \tag{10}$$

Clearly, this expression does not hold for porosity values below 8%, hence, a mesoporosity of 10% is used as the lower bound in the grain simulations; as shown later, this limit is never reached in the simulations. The Knudsen diffusivity accounts for the size of the mesopores, whereas the binary molecular diffusivity is calculated using the method of Fuller et al. [43]. The boundary conditions needed to solve equation (8) are:

$$p_{is} = p^s_{is} \text{ at } \xi_g = R_{grain} \tag{11a}$$

$$\frac{dp_{is}}{d\xi_g} = 0 \text{ at } \xi_g = 0 \tag{11b}$$

In Eq. (11a), R_{grain} is the radius of the grain. The density of the mesoporous grain is given by:

$$\rho_g = \rho_z\varepsilon_z + \rho_{Si}(1 - \varepsilon_z) \tag{12}$$

In Eq. (12), ρ_z is the density of the zeolite, ρ_{Si} is the density of the purely mesoporous silica, and ε_z is the volume fraction of zeolite in the composite. The effectiveness factor at the grain level can be calculated as:

$$\eta_g = \frac{3}{R^3_{grain}}\frac{\int_0^{R_{grain}} r(p_{Es}, p_{Bs}, p_{EBs})\xi_g^2 d\xi_g}{r(p^s_{Es}, p^s_{Bs}, p^s_{EBs})} \tag{13}$$

The volume-integrated reaction yield is obtained by integrating the reaction rate over the entire grain volume as:

$$\text{Yield} = 4\pi\int_0^{R_{grain}} r(p_{Es}, p_{Bs}, p_{EBs})\xi_g^2 d\xi_g \tag{14}$$

In addition, the reaction yield can be normalized by the volume-integrated reaction yield from a zeolite crystal of the same radius as the grain, as shown below:

$$\text{Scaled yield} = \frac{\int_0^{R_{grain}} r(p_{Es}, p_{Bs}, p_{EBs})\xi_g^2 d\xi_g}{\int_0^{R_z = R_{grain}} r(p_{Es}, p_{Bs}, p_{EBs})\xi_z^2 d\xi_z} \tag{15}$$

The resulting scaled yield is a useful metric to quantify the superior catalytic activity of the mesoporous zeolite composite over the pure zeolite.

Please cite this article in press as: S.M. Rao et al., Surface barriers as dominant mechanism to transport limitations in hierarchically structured catalysts – Application to the zeolite-catalyzed alkylation of benzene with ethylene, Chem. Eng. J. (2017), http://dx.doi.org/10.1016/j.cej.2017.04.015

2.3. Diffusion and reaction within a hierarchically structured catalyst pellet

At the pellet scale, the equation for diffusion and reaction of each component is written in a similar manner to the grain-level equations as:

$$\frac{1}{\xi_p^2}\frac{d}{d\xi_p}\left(\xi_p^2\frac{D_{E,i}}{R_g T_s}\frac{dp_{is}}{d\xi_p}\right) = \nu_i r \eta_g (p_{Es}, p_{Bs}, p_{EBs})\rho_p \tag{16}$$

In Eq. (16), ξ_p is the radial coordinate along the pellet radius, $D_{E,i}$ is the effective diffusivity of species i in the pellet, accounting for the macropores in between the grains, and ρ_p is the density of the catalyst pellet, which accounts for the macroporosity ε_{sM} as:

$$\rho_p = \rho_g(1-\varepsilon_{sM}) \tag{17}$$

Diffusion limitations within the mesoporous zeolite composite grains are included in the pellet-scale equations by means of the grain-level effectiveness factor. As will be discussed further on, for the range of zeolite weight fractions simulated, there are no internal diffusion limitations within the grains, because the size of the grains is small enough that the mesopores are sufficient to efficiently transport reactant and product molecules to and from the zeolite crystals. However, this is not the case for the pure zeolite pellet which contains only crystals and macropores. The size of the grains can be calculated from the properties of the macropore network, by assuming a geometry for the catalyst pellet and the grains, such as that given by Rao and Coppens [17] or Wang et al. [44]. If the catalyst is assumed to consist of spherical mesoporous silica/zeolite grains which randomly intersect and overlap with each other, and with macropores in between the grains, the radius of these grains can be calculated as (see Rao and Coppens [17]):

$$R_{grain} = \frac{-3}{2}R_M \ln \varepsilon_{sM} \tag{18}$$

Alternatively, using the square geometry discussed by Wang et al., the size of the mesopore-zeolite domains can be calculated as [44]:

$$R_{grain} = \frac{R_M}{\varepsilon_{sM}}\left(1-\varepsilon_{sM}+\sqrt{1-\varepsilon_{sM}}\right) \tag{19}$$

In Eqs. (18) and (19), R_M is the radius of the macropores. The values of the grain radius, calculated from either equation (18) or (19), along with the partial pressure profiles along the radius of the pellet, are used to solve the grain-scale problem described in Section 2.2. The effective diffusivity in the macroporous pellet is calculated using the Bosanquet approximation, correcting for the porosity and the tortuosity factor, as described previously. The boundary conditions for the pellet-scale equations are:

$$p_{is} = p_{is}^s \text{ at } \xi_p = R_{pellet} \tag{20a}$$

$$\frac{dp_{is}}{d\xi_p} = 0 \text{ at } \xi_p = 0 \tag{20b}$$

In Eq. (20a), R_{pellet} is the radius of the pellet. Once again, the effectiveness factor at the pellet scale can be calculated as:

$$\eta_p = \frac{3}{R_{pellet}^3}\frac{\int_0^{R_{pellet}} r(p_{Es}, p_{Bs}, p_{EBs})\xi_p^2 d\xi_p}{r(p_{Es}^s, p_{Bs}^s, p_{EBs}^s)} \tag{21}$$

The volume integrated reaction yield is also calculated as:

$$\text{Yield} = 4\pi\int_0^{R_{pellet}} r(p_{Es}, p_{Bs}, p_{EBs})\rho_g(1-\varepsilon_{sM})\xi_p^2 d\xi_p \tag{22}$$

The macroporosity is varied in order to maximize the reaction yield. The macropore diameter is not optimized for reasons explained in Section 3.

2.4. Reactor scale model

In order to compare the catalytic properties of different hierarchically structured zeolites at the reactor scale, the catalyst pellet model, described in Section 2.3 was coupled to a one-dimensional, isothermal fixed bed reactor model. The experiments with the zeolite composites are described in Section 4. The pressure drop across the experimental catalyst bed is not significant, as verified by a calculation using Ergun's equation. Thus, only a material balance is needed, given by [41]:

$$\frac{-dF_i}{dz} = \nu_i \eta_p r \rho_B \Omega \tag{23}$$

In Eq. (23), F_i is the molar flowrate of species i, z is the axial coordinate along the reactor length, ρ_B is the density of the catalyst, defined per unit volume of the reactor, and Ω is the cross-sectional area of the reactor. The boundary condition needed to solve equation (23) is:

$$F_i = F_{i,0} \text{ at } z = 0 \tag{24}$$

In Eq. (24), $F_{i,0}$ is the inlet molar flowrate of species i. At every step in the integration of the reactor model, the molar flowrates of the reactants and products are used to calculate the partial pressures at the external surface of the catalyst pellet, as described by Coppens and Froment [45]:

$$p_{is}^s = \left(\frac{F_i}{\sum_{i=1}^3 F_i}\right)p_t \tag{25}$$

The total pressure is denoted by p_t in Eq. (25). The partial pressures, in turn, are used in the solution of the boundary value problem for the catalyst pellet, from which the effectiveness factor at the pellet scale, η_p, can be calculated. Finally, the conversion of ethylene and benzene are obtained from the exit molar flow rates as:

$$x_i = 1.0 - \frac{(F_i)_{z=L}}{F_{i,0}} \tag{26}$$

3. Simulation

The set of equations described in Section 2 were converted to the corresponding dimensionless forms and solved using the software package Athena Visual Studio. The finite difference method with a sufficiently large number of grid points was used in the discretization of the ordinary differential equations for the catalyst pellet, grain and zeolite crystal models. For the reactor model, a damped Newton algorithm is implemented in the software itself. For the simulation, the values of the reaction rate constants, adsorption constants and diffusion coefficients are taken from Hansen et al. [38]. In particular, using the data reported at three different temperatures (603, 653 and 703 K), the temperature dependence could be regressed assuming an Arrhenius relationship for both the kinetic and adsorption constants. The process conditions, such as temperature, pressure and the molar benzene to ethylene ratio are also taken from Hansen et al. [38]. The Brønsted acid site concentration is calculated assuming one acid site per channel intersection in zeolite ZSM-5. Considering that the MFI framework has 96 possible locations for substitution of silicon atoms by aluminum atoms per unit cell and that each Al atom corresponds to one acid site, 96/24 = 4 acid sites per unit cell are taken into account. This would, thus, be valid for ZSM-5 zeolites

Please cite this article in press as: S.M. Rao et al., Surface barriers as dominant mechanism to transport limitations in hierarchically structured catalysts – Application to the zeolite-catalyzed alkylation of benzene with ethylene, Chem. Eng. J. (2017), http://dx.doi.org/10.1016/j.cej.2017.04.015

with a molar Si/Al ratio of 24. For the simulation of the silica-zeolite composites, the properties of the purely mesoporous silica phase are taken from nitrogen adsorption analysis of the silica material employed in the experiments. The density of solid silica was taken to be that of amorphous fused silica [46]. The mesopore diameter in the composite material is determined by the synthesis approach, and can be tuned by varying the non-templating structure directing agent employed (see Wang et al. [47]). The macropore diameter is also subject to the pelletization constraints, and it may not be possible to tune the macropore diameter beyond a certain size, without sacrificing a property such as the crush strength or the pellet size. Mercury porosimetry was used to determine the average macropore diameter of the different mesoporous silica/zeolite composite pellets used in the reactor experiments, which was 1.5 μm. All simulations were run on a Dell Latitude laptop with a 2.7 GHz Intel i5 processor and 8 GB of RAM. The computer code for the pellet simulations is packaged as an object file and is used in the reactor simulations. Typical run times were of the order of tens of seconds for the pellet simulations, and around twenty seconds for the reactor simulations. The simulation parameters are reported in Table 1. Finally, it must be noted that optimization was carried out through different parametric studies, rather than through a numerical optimization routine.

4. Results and discussion

4.1. Effectiveness factor for a single zeolite crystal

Fig. 2 shows the effectiveness factor for a single zeolite crystal as a function of the zeolite crystal radius over a fairly broad range (50–400 nm). In previous work [14–17], we have shown that, in the optimal hierarchical structures, diffusion limitations vanish in the catalytically active regions of the catalyst (mesoporous regions in hierarchical meso-macroporous alumina, for example). We can use this insight to determine the largest size of the zeolite crystal that can be incorporated into the hierarchical structure while maintaining an effectiveness factor as close to 1 as possible. If we set the criterion on the effectiveness factor to be >95%, then Fig. 1 shows that the zeolite crystals must be smaller than 120 nm in radius. Synthesis of zeolite crystals of such a size, either via direct synthesis [48] or via single-pot synthesis of mesoporous silica/zeolite composites [4] can be achieved by tuning the hydrothermal synthesis time. For example, Wang et al. [4] have demonstrated the synthesis of mesoporous ZSM-5 composites in which the zeolite crystals show a size range between 150 and 250 nm in diameter. For further discussions, the zeolite crystal radius is kept constant at 120 nm, unless explicitly mentioned otherwise.

Table 1
Simulation parameters. The kinetic constants correspond to a temperature of 653 K.

Parameter	Value	Units
Total pressure	506625	Pa
Temperature	653	K
Benzene: Ethylene molar ratio	5:1	mol/mol
Partial pressure of ethylbenzene at the external surface of the catalyst	35	Pa
Forward rate constant	696	1/s
Reverse rate constant	0.137	1/s
Number of acid sites per unit cell	4.0	1/unit cell
Density of pure silica	2200	kg/m^3_{solid}
Specific mesopore volume	0.93	cm^3_f/g silica
Mesopore diameter	6.0	nm
Macropore diameter	1.5	μm
Pellet diameter	2.0	mm

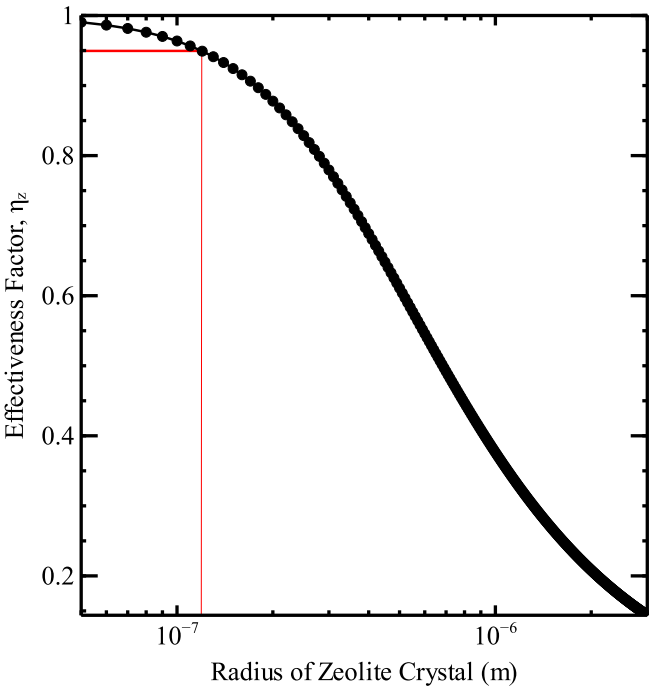

Fig. 2. Effectiveness factor of a single ZSM-5 crystal as a function of the radius of the crystal, for the process conditions shown in Table 1.

4.2. Effectiveness factor for a single mesoporous silica/zeolite composite grain

Fig. 3 shows the effectiveness factor obtained from a single mesoporous silica/zeolite composite grain as a function of the weight fraction of zeolite. The grain size was calculated using the macropore diameter in Table 1 and a range of macroporosity

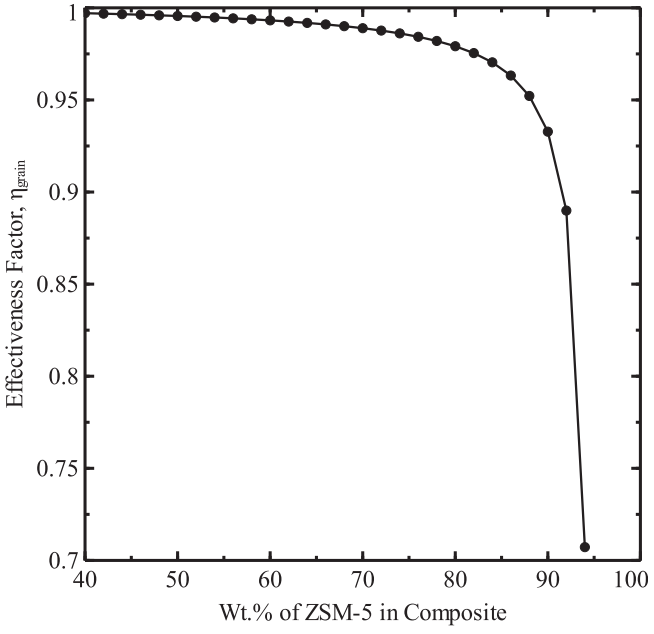

Fig. 3. Effectiveness factor of a single mesopore-zeolite composite grain as a function of the weight fraction of zeolite in the composite.

Please cite this article in press as: S.M. Rao et al., Surface barriers as dominant mechanism to transport limitations in hierarchically structured catalysts – Application to the zeolite-catalyzed alkylation of benzene with ethylene, Chem. Eng. J. (2017), http://dx.doi.org/10.1016/j.cej.2017.04.015

values substituted into Eqs. (18) and (19). For example, assuming a macroporosity of 10% and a macropore diameter of 1.5 μm yields a grain radius of about 2.6 μm from Eq. (18) and 14 μm from Eq. (19). Assuming a macroporosity of 60% yields a grain radius of about 0.6 μm and 1.3 μm, respectively. It is clear that different geometric representations of the pore space can result in significantly different values for the geometric properties of the pore space architecture. Catalyst pellets formed by pelletization are more likely to contain grains in the form of overlapping agglomerates [49], rather than in a nicely ordered geometric arrangement, as assumed by Wang et al. [43]. However, it is equally important to ensure that the continuum approach is valid over the entire range of macroporosities and grain radii. Since the grains contain zeolite crystals of a known size, it is possible to set a lower bound on the grain radius such that the ratio of the grain radius to the zeolite crystal radius is large enough for a continuum approach to hold within the grain. If we choose the ratio of radii to be equal to 10, then the lower bound on the grain radius is 1.2 μm for zeolite crystals of a radius of 120 nm. Clearly, only Eq. (19) allows for this lower bound to be satisfied over the entire range of macroporosities for the fixed macropore diameter of 1.5 μm. Therefore, Eq. (19) is retained in order to calculate the grain radius in all further simulations. For the grain-level optimization, the radius is chosen to be 14 μm. The zeolite weight fraction is varied over a wide range to determine the maximum possible zeolite content that results in a large value of the volume-integrated reaction yield, while maintaining a grain level effectiveness factor close to 1.

Fig. 3 shows that the effectiveness factor is greater than 95% even when the zeolite weight content is as high as 80 wt.%. The mesoporosity corresponding to this weight fraction is about 26%, which means that the tortuosity factor calculation is still valid. Moreover, Reyes and Iglesia [49] have shown that the percolation threshold for pore space of porous catalysts can be as low as 5%, which is close to the lower bound on the porosity for the calculation of the tortuosity factor in Eq. (10).

Fig. 4 shows the scaled yield (see Eq. (15)) from mesoporous silica/zeolite composites as a function of their zeolite weight percentage. Clearly, the composites are superior in catalytic activity to the pure zeolite crystal, which can be attributed to the enhanced transport through the mesopores, in addition to the lack of diffusion limitations within the zeolite crystals. It must be pointed out that a pure zeolite crystal with the same radius as that of the grain has an effectiveness factor of only 5%, whereas the composites have an effectiveness factor greater than 70% over the entire range of zeolite weight fractions simulated (up to 95%, see Fig. 3). Thus, the composites are superior to the pure zeolite from the standpoint of catalyst utilization as well. Fig. 4 shows a maximum with respect to the zeolite weight fraction around 90 wt.%, beyond which the yield and the effectiveness factor decrease significantly, due to the low mesoporosity and high tortuosity factor. From these grain-level simulations, grains with a weight fraction of 0.8 (80 wt.%) of zeolite crystals of radius 120 nm and a mesoporosity of 0.26 (26%) were chosen for the pellet-scale simulations.

4.3. Optimization at the pellet scale

The optimization at the pellet scale is targeted toward finding the optimum macroporosity for which the volume integrated reaction yield from a mesoporous silica/zeolite composite pellet is maximized over the corresponding yield from a pure zeolite pellet. In the latter case, the catalyst contains only macropores that separate the zeolite crystals. The macropore diameter is not optimized since mercury porosimetry of catalyst pellets for the different composites synthesized during the course of this work showed the same average diameter. Thus, only the macroporosity is varied, which influences the calculation of the grain radius through Eq. (18). Since the zeolite crystals are small enough that there are no internal diffusion limitations, the simulation of the hierarchical model is simplified by assuming a zeolite-level effectiveness factor of 1. Thus, only the grain and pellet scale equations need to be solved.

Fig. 5 shows the variation in reaction yield at the pellet scale with respect to the macroporosity for a hierarchically structured catalyst pellet and a pure ZSM-5 pellet. An upper limit of 70% on the macroporosity is assumed in the simulations, since large macroporosities may lead to poor mechanical properties in the final pelletized catalyst. As mentioned previously, the macropore

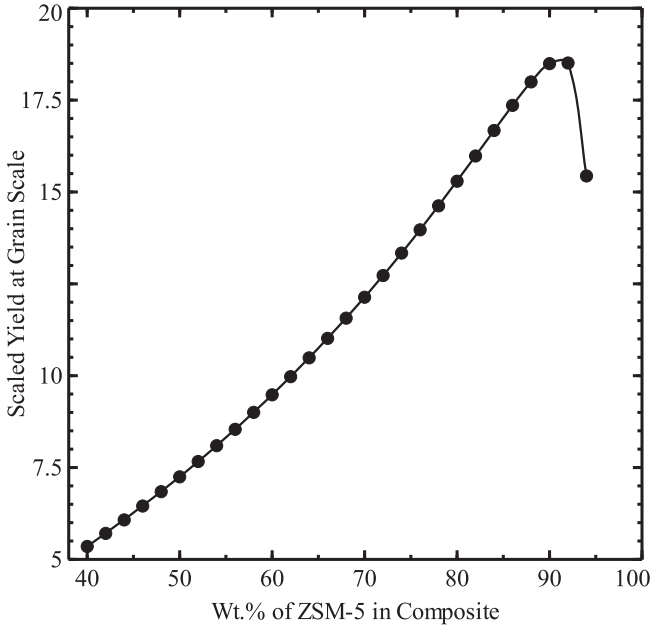

Fig. 4. Volume-integrated reaction yield from a single mesoporous silica/zeolite composite grain as a function of the weight fraction of zeolite in the composite.

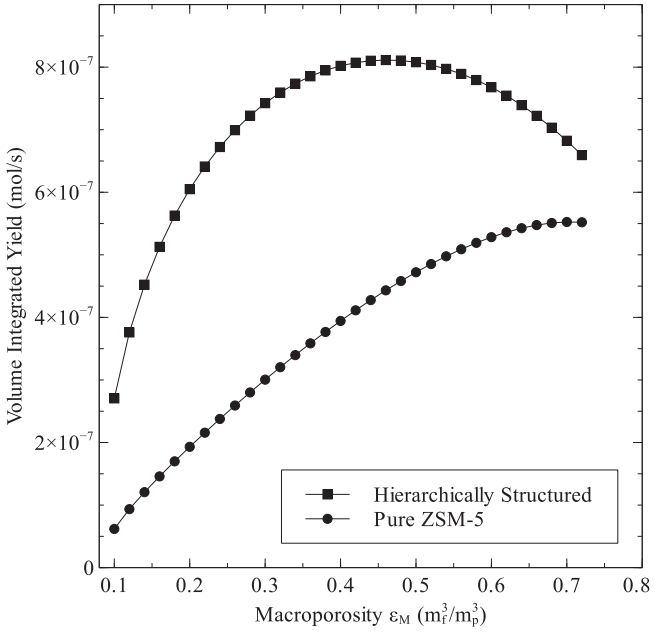

Fig. 5. Variation of the reaction yield from a hierarchically structured zeolite catalyst pellet, and a pure zeolite catalyst pellet (without mesopores), as a function of the macroporosity in the pellet. All simulation conditions correspond to Table 1.

Please cite this article in press as: S.M. Rao et al., Surface barriers as dominant mechanism to transport limitations in hierarchically structured catalysts – Application to the zeolite-catalyzed alkylation of benzene with ethylene, Chem. Eng. J. (2017), http://dx.doi.org/10.1016/j.cej.2017.04.015

diameter is fixed at 1.5 μm. The maximum yield from the hierarchical structure is nearly twice the corresponding yield from the pure ZSM-5 pellet, corresponding to a macroporosity of 46%. The optimized meso- plus macroporosity in this case is calculated as:

$$\varepsilon_t = \varepsilon_{sM} + \varepsilon_{sm}(1 - \varepsilon_{sM}) = 0.46 + 0.26(1 - 0.46) = 0.6\,\mathrm{m_f^3/m_p^3} \quad (27)$$

The rationale for optimizing the total meso- plus macroporosity is as follows: while synthesis conditions can be fine-tuned to obtain the desired mesoporosity in a zeolite composite, it might be harder to tune the macroporosity, since the desired properties of the pellet, such as crush strength, or the conditions of the pellet-forming process may not afford a wide range of control. Optimizing the total meso- plus macroporosity provides flexibility in tuning the synthesis conditions to achieve a desired mesoporosity, if macroporosity cannot be controlled easily. The pure ZSM-5 pellet does not show a maximum in reaction yield with respect to the macroporosity, because, at lower macroporosities, the calculated crystal radius from Eqs. (18) and (19) is large (please see the discussion in Section 4.2), implying the existence of strong intracrystalline diffusion limitations. By increasing macroporosity for a fixed macropore diameter, the crystal radius decreases, allowing for increased utilization of the zeolite and a corresponding increase in the reaction yield. Beyond a certain macroporosity, the improved mass transport within the smaller zeolite crystals is offset by the reduced amount of catalyst, and the reaction yield decreases. Fig. 5 comprehensively demonstrates that by optimizing the grain level structure in a hierarchical zeolite, it is possible to limit the extent of diffusion limitations to the macropores, whereas in the case of a pure ZSM-5 pellet, the intracrystalline diffusion limitations determine the overall performance of the catalyst.

4.4. Comparison with experiments and influence of surface barriers

The previous sub-sections have provided insight into the properties of an optimal hierarchical pore structure to minimize diffusion limitations in the alkylation of benzene with ethylene. It is equally important to complement such modeling studies with experimental data to ascertain if these computational approaches can help guide the synthesis of more active catalysts. Therefore, a series of composites consisting of mesoporous silica (Davisil grade 633, Sigma Aldrich) and commercial zeolite ZSM-5 (Süd-Chemie AG, Si/Al molar ratio = 55) with varying zeolite content was synthesized by physically mixing together the zeolite and mesoporous silica phases, and then pressing the composites into pellets that were sieved to a size range of 280–313 μm. While composites of zeolite crystals and meso/macroporous material can be synthesized in a variety of ways, which produce varying final composite structures [23], it was decided to focus on a single type of zeolite composite, which is easily produced by physically mixing together zeolite crystals with a mesoporous silica material. The pelletization process introduces macroporosity into the final materials. These pellets were subsequently tested in an isothermal fixed bed reactor operated at the conditions shown in Table 2. From SEM analysis of the zeolite crystals, an average sphere diameter of 3.6 μm was assumed for all the simulations. The composites and pellets were characterized using SEM, nitrogen sorption and mercury porosimetry. Interestingly, mercury porosimetry showed that the macroporosity of the pellets on a unit zeolite mass basis remained constant, and hence, is reported as such in Table 2. The catalyst preparation and characterization methods, as well as the fixed bed reactor experiments, will be described in more detail in a forthcoming publication. The catalytic activity of the composites was quantified by measuring the experimental conversion of ethylene and benzene to ethylbenzene. To compare with these experiments, reactor simulations of the zeolite composite pellets were carried out at the conditions listed in Table 2.

Table 2
Properties of mesopore-zeolite composites and conditions for fixed bed reactor experiments. The compositions correspond to the inlet conditions.

Parameter	Value	Units
Total pressure	1	Bar
Temperature	623	K
Mass of catalyst	0.3	g
Void fraction of catalyst bed	0.38	m_f^3/m_r^3
WHSV (total mass feed basis)	10	$kg_{(C2H4+C6H6)}/kg_{pellet}/h$
Mole fraction of nitrogen (inert)	0.2	mol/mol
Mole fraction of ethylene	0.2	mol/mol
Mole fraction of benzene	0.6	mol/mol
Total molar flow at reactor inlet	1.56×10^{-5}	mol/s
Pellet diameter	280	μm
ZSM-5 crystal diameter	3.6	μm
Macroporosity of pellet	0.675	$cm_f^3/g_{zeolite}$
Macropore diameter	1.5	μm
Mesopore diameter	6	nm
Brønsted acid site density	4	acid sites/unit cell

While the previous sections have focused on a hierarchical approach to describe diffusion and reaction within the catalyst pellet, such an approach could not be directly used for comparison with the experimental data. This is due to the large size of the zeolite crystals, which violates the requirements for the validity of the continuum approach, as defined in Section 4.2. Additionally, the synthesis method employed for the composites produces agglomerates of zeolite crystals which may or may not contain agglomerates of the mesoporous silica phase. In this situation, a better approach to modeling the pore structure of the catalyst is to assume the zeolite and silica phases to be two separate continua. The macropores are assumed to be present in between the two phases, and the effective diffusivities are computed by combining diffusion through the macro- and mesopores, using the Wakao and Smith model [8]. However, reactor simulations which considered diffusion only through the macropores yielded ethylene and benzene conversions that were not significantly different from the conversions calculated assuming the Wakao and Smith model. This observation can be explained as follows: at low zeolite weight fractions, the macroporosity of the pellet is also low because the macroporosity on a unit zeolite mass basis is constant. Hence, transport occurs predominantly through the mesoporous phase. However, the low zeolite weight fraction also translates into a lower volumetric catalytic activity, and hence, the performance is limited by kinetics. At higher zeolite weight fractions, the macroporosity is also correspondingly higher, and transport through the macropores dominates over the mesopores. Therefore, all the pellet scale simulations were carried out assuming diffusion through the macropores alone, with the mesoporous silica phase simply acting as a diluent.

The comparison between the experiments and simulations, plotted in Fig. 6, shows an unexpected result: the simulations predict an increasing conversion of ethylene with increasing zeolite content in the mesopore-zeolite composites, whereas the experiments show a maximum in ethylene conversion at around 40 wt. % zeolite in the composite. The experimental results are somewhat surprising, because they imply a maximum in conversion due to diffusion limitations at the pellet scale. For zeolite crystals of diameter 3.6 μm employed in the experiments, the zeolite level effectiveness factor at these experimental process conditions is around 55%. The low effectiveness factor at the zeolite crystal scale, in combination with the small diameter of the pellets, should not result in any diffusion limitations at the pellet scale. Indeed, standalone pellet-level simulations incorporating the zeolite crystals and mesoporous phases of the synthesized composites show a

Please cite this article in press as: S.M. Rao et al., Surface barriers as dominant mechanism to transport limitations in hierarchically structured catalysts – Application to the zeolite-catalyzed alkylation of benzene with ethylene, Chem. Eng. J. (2017), http://dx.doi.org/10.1016/j.cej.2017.04.015

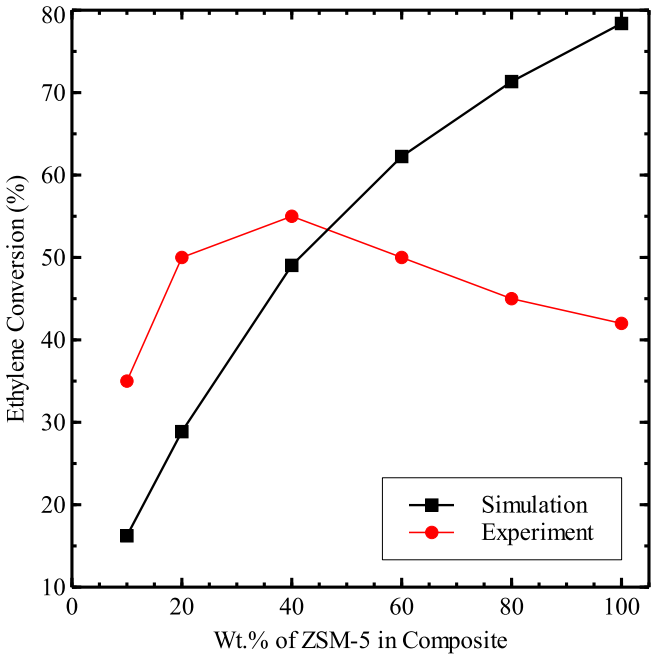

Fig. 6. Comparison of ethylene conversion from different zeolite composites. The simulation data are obtained assuming no surface barrier limitations, under the conditions listed in Table 2.

pellet scale effectiveness factor close to 1. Thus, it appears that there is some other factor other than diffusion limitations within the macropores or the zeolite crystals that is limiting performance, since the present model accounts for both these factors.

If one examines closely the SEM images of the prepared composites, it appears that the zeolite crystals tend to aggregate close to each other, rather than being uniformly distributed in the mesoporous matrix. The tendency of the crystals to aggregate increases with increasing zeolite content. Fig. 7 shows an SEM image of a composite containing 40 wt.% ZSM-5; it can be clearly seen that the zeolite crystals form aggregates separated by the mesoporous silica phase. This aggregation, in turn, can induce surface barriers due to blockage of the external surface of the zeolite crystals. It is, therefore, important to determine if surface barriers, rather than intrapellet diffusion limitations, are responsible for the trends displayed by the experimental data. Accounting for surface barriers requires the use of Eq. (6c) in the solution of the zeolite level equations. To use Eq. (6c), the surface permeabilities of the different composite materials need to be known. Unfortunately, the literature contains limited information on this aspect. Kärger and coworkers [29] reported surface permeabilities in the range of 10^{-7} to 10^{-9} m/s for methanol uptake in SAPO-34 at very low pressures (0–3 mbar). Therefore, this range of values was used as a starting point and the surface permeability value for each composite was tuned until the reactor simulation results were comparable to the experimental data. The tuned surface permeabilities are reported in Table 3, and a comparison between the experiments and the model, after accounting for surface barriers, is shown in Fig. 8. It must be pointed out that, since surface barriers further reduce the rate of reaction at the zeolite crystal level, the extent of diffusion limitations at the pellet scale is further reduced, and, thus, single-pellet simulations again show an effectiveness factor close to 1. Therefore, for the solution of the pellet-scale equations in the reactor simulation, the partial pressure profiles at the reactor level could be used directly in the Neumann boundary condition for the solution of the zeolite crystal level equations. The reaction rate at the zeolite crystal level was then integrated over the entire pellet volume, after correcting for the weight fraction of the zeolite in the composite, and used as the source term in the reactor model. Table 3 also shows that the surface permeability of the composite had to be decreased with increasing zeolite content, in order to match the experimental data. This is probably an indication that the extent of agglomeration of the zeolite crystals increases with increasing zeolite content, leading to increased transport along the grain boundaries between the zeolite crystals. Additionally, the same surface permeability value is assumed for all three species in this system, for each zeolite composite, primarily due to the lack of information about this parameter in the literature.

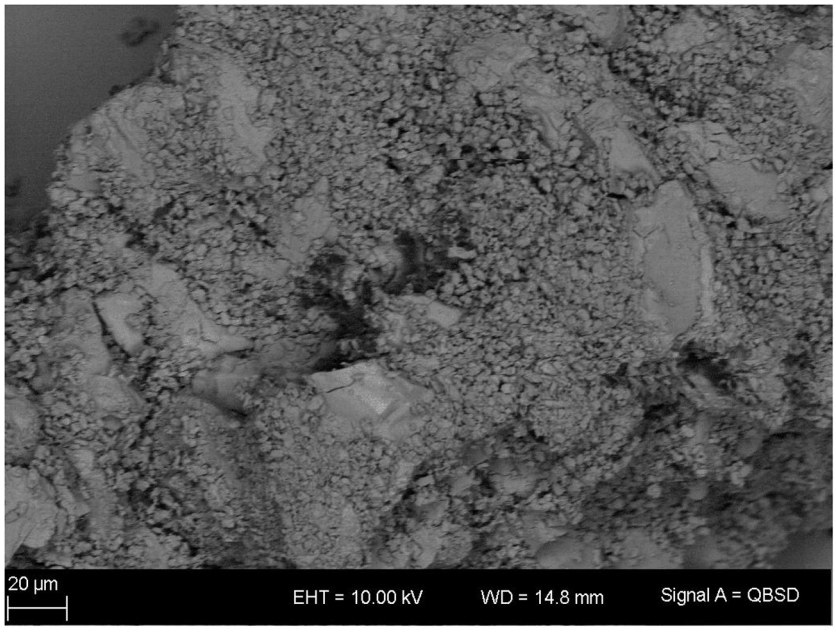

Fig. 7. SEM image of a single catalyst pellet containing 40 wt.% ZSM-5 and 60 wt.% mesoporous silica. The ZSM-5 crystals form agglomerates, which surround the mesoporous silica phase (appearing as large, continuous clumps: mesopores are not visible at this scale).

Please cite this article in press as: S.M. Rao et al., Surface barriers as dominant mechanism to transport limitations in hierarchically structured catalysts – Application to the zeolite-catalyzed alkylation of benzene with ethylene, Chem. Eng. J. (2017), http://dx.doi.org/10.1016/j.cej.2017.04.015

Table 3
Values of the surface permeability of the different mesopore-ZSM-5 composites used in the reactor simulations.

Wt. % of ZSM-5	Surface Permeability, α (m/s)
10	5×10^{-5}
20	5×10^{-5}
40	1×10^{-5}
60	2×10^{-6}
80	8×10^{-7}
100	5×10^{-7}

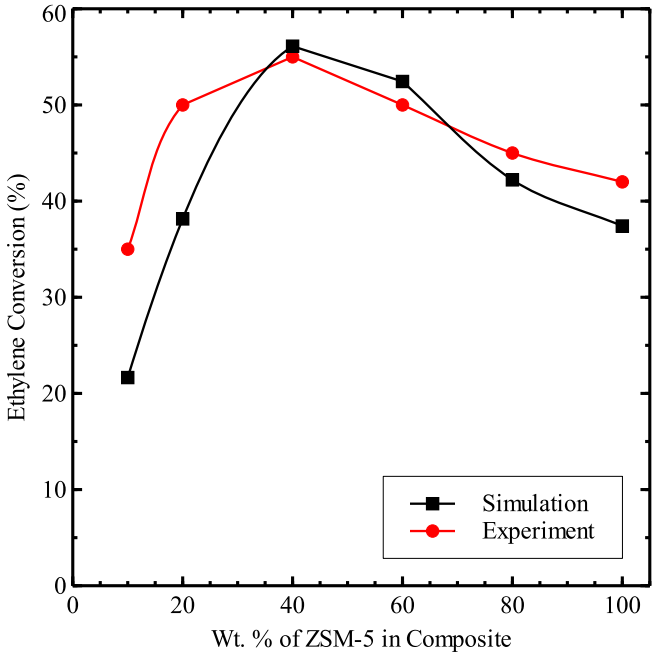

Fig. 8. Comparison of ethylene conversion from different zeolite composites. The simulation data are obtained assuming surface barrier limitations, under the conditions listed in Table 2. The surface barrier permeability values for each composite are listed in Table 3.

Fig. 8 clearly shows that accounting for surface barriers leads to much better qualitative and quantitative agreement between the model and experiments. The maximum deviation is observed for the composites containing 10 and 20 wt.% ZSM-5. Fig. 8 demonstrates experimentally and theoretically, for the first time, the possible role of surface barriers in limiting the performance of hierarchically structured porous catalysts. However, it must be emphasized that these surface barriers may actually be lumping together multiple effects which are collectively responsible for the observed experimental data. Recently, Bai et al. [50] demonstrated via molecular dynamics simulations that the self-diffusivity of n-hexane in hierarchically structured pentasil type zeolites is much lower than in the case of pure MFI. They rationalized these results on the basis that, at low adsorbed loadings of n-hexane, molecules diffuse primarily through the intracrystalline pathways, and exhibit similar behavior to diffusion in pure MFI. At higher adsorbed phase loadings, the straight and sinusoidal channels of a zeolite crystal are saturated, and the molecules tend to diffuse primarily through the mesopores, thus leading to the observations of a higher, effective self-diffusivity. For the benzene alkylation system studied here, the low total pressure and comparatively lower temperature are both conditions that could correspond to the low adsorbed phase loading scenario described by Bai et al. [50]. At the pellet scale, there are no diffusion limitations; hence, it is possible that molecules diffuse entirely through the zeolite crystals, and the extent of zeolite crystal agglomeration leads to hopping between adjoining zeolite crystals via grain boundaries, rather than via diffusion in the meso- and macropores. The maximum in the ethylene conversion with respect to zeolite weight fraction in the pellet could then be explained by a trade-off between increased zeolite crystal agglomeration, which leads to more tortuous diffusion pathways, and the availability of sufficient amounts of active catalyst for reaction. Thus, there are a number of factors, such as pore blockage, zeolite crystal agglomeration, and activation energy barriers within the zeolite crystal that can possibly explain the experimental observations on a fundamental level, and are lumped as surface barriers in the continuum model. The simulations suggests that the impact of these barriers becomes more significant and the surface permeability decreases with increasing zeolite weight fraction.

These findings also highlight the need to include the effect of surface barriers in the computer-aided rational design of catalysts. For example, single-pellet optimization studies that account for surface barriers will show the reduced sensitivity of the volume-integrated reaction yield to the pellet macroporosity. This is a result of the lower volume-integrated yield at the zeolite crystal scale, which translates into a lower effective rate of reaction at the pellet scale. Thus, although the zeolite crystals may not be internally diffusion limited, owing to their small size, the surface barriers nonetheless impose transport limitations, and the macropore network properties are no longer as crucial in structuring the catalyst architecture in an optimal manner for maximum reaction yield.

5. Conclusion

The total meso- plus macroporosity of a hierarchically structured composite of microporous zeolite and mesoporous silica must be optimized to maximize the volume-integrated reaction yield of the diffusion limited ethylation of benzene beyond that of pure zeolite pellets, which contain only zeolite crystals separated by macropores. The calculations presented here also show the need to characterize the composites at different stages in the catalyst manufacturing steps, so that the textural parameters can be properly accounted for in the modeling and optimization work. Surface barriers, if important, can mask the effect of intracrystalline diffusion limitations, especially for small zeolite crystals, and this may lead to erroneous interpretation of experimental data. Surface barriers can lead to lower volume-integrated reaction yields from pellets formed of single zeolite crystals. The global reaction rate at the scale of the catalyst pellet is comparatively lower when surface barriers are present, thus leading to a lower sensitivity in the optimum yield, with respect to macroporosity. The experimental determination of zeolite surface permeabilities under reaction conditions thus becomes important to understand the limitations imposed by surface barriers, so that the latter can be properly accounted for in catalyst and reactor design. This is a new experimental challenge, and our work demonstrates the practical importance of such measurements in the context of catalytic reaction engineering.

Acknowledgement

The authors gratefully acknowledge financial support for this work from Synfuels China and the UK EPSRC (EP/K038656/1) for supporting the Center for Nature Inspired Engineering at University College London via a "Frontier Engineering" award. Kaiqiao Wu from UCL is acknowledged for the mercury porosimetry measurements. The authors also acknowledge helpful discussions with Prof. Frerich J. Keil of the Hamburg University of Technology, Germany.

References

[1] A.T. Bell, M. Head-Gordon, Quantum mechanical modeling of catalytic processes, Annu. Rev. Chem. Biomol. Eng. 2 (2011) 453–477.
[2] I.E. Wachs, K. Routray, Catalysis science of bulk mixed oxides, ACS Catal. 2 (2012) 1235–1246.
[3] E. Jeroro, K. Vanden Bussche, The role of characterization and modeling techniques in fostering the era of computer-based catalyst and reactor design, Curr. Opin. Chem. Eng. 13 (2016) 186–192.
[4] J. Wang, J.C. Groen, W. Yue, W. Zhou, M.-O. Coppens, Single-template synthesis of zeolite ZSM-5 composites with tunable mesoporosity, Chem. Commun. 4653–4655 (2007).
[5] J. Wang, J.C. Groen, W. Yue, W. Zhou, M.-O. Coppens, Facile synthesis of ZSM-5 composites with hierarchical porosity, J. Mater. Chem. 18 (2008) 468–474.
[6] J. Wang, W. Yue, W. Zhou, M.-O. Coppens, TUD-C: a tunable, hierarchically structured mesoporous zeolite composite, Microporous Mesoporous Mater. 120 (2009) 19–28.
[7] J.J. Carberry, The micro-macro effectiveness factor for the reversible catalytic reaction, AIChE J. 8 (1962) 557–558.
[8] N. Wakao, J.M. Smith, Diffusion in catalytic pellets, Chem. Eng. Sci. 17 (1962) 825–834.
[9] N. Örs, T. Dogu, Effectiveness of bidisperse catalysts, AIChE J. 25 (1979) 723–725.
[10] L.L. Hegedus, Catalyst pore structure by constrained nonlinear optimization, Ind. Eng. Chem. Prod. Res. Dev. 19 (1980) 533–537.
[11] B.D. Kulkarni, V.K. Jayaraman, L.K. Doraiswamy, Effectiveness factors in bidisperse catalysts—the general nth order case, Chem. Eng. Sci. 36 (1981) 943–945.
[12] C.J. Pereira, J.E. Kubsh, L.L. Hegedus, Computer-aided design of catalytic monoliths for automobile emission control, Chem. Eng. Sci. 43 (1988) 2087–2094.
[13] J.W. Beeckman, L.L. Hegedus, Design of monolith catalyst for power plant NOx emission control, Ind. Eng. Chem. Res. 30 (1991) 978–983.
[14] G. Wang, M.-O. Coppens, Calculation of the optimal macropore size in nanoporous catalysts and its application to DeNOx catalysis, Ind. Eng. Chem. Res. 47 (2008) 3847–3855.
[15] G. Wang, M.-O. Coppens, Rational design of hierarchically structured porous catalysts for autothermal reforming of methane, Chem. Eng. Sci. 65 (2010) 2344–2351.
[16] S.M. Rao, M.-O. Coppens, Mitigating deactivation effects through rational design of hierarchically structured catalysts: application to hydrodemetalation, Ind. Eng. Chem. Res. 49 (2010) 11087–11097.
[17] S.M. Rao, M.-O. Coppens, Increasing robustness against deactivation of nanoporous catalysts by introducing an optimized hierarchical pore network—application to hydrodemetalation, Chem. Eng. Sci. 83 (2012) 66–76.
[18] F.J. Keil, C. Rieckmann, Optimization of catalyst pore structures, Hung. J. Ind. Chem. 21 (1993) 277–286.
[19] F.J. Keil, C. Rieckmann, Optimization of three-dimensional catalyst pore structures, Chem. Eng. Sci. 49 (1994) 4811–4822.
[20] J. Hinderer, F.J. Keil, Diffusion and reaction in composite catalysts, Hung. J. Ind. Chem. 23 (1995) 207–213.
[21] C. Rieckmann, T. Duren, F.J. Keil, Interaction of kinetics and geometric structure of pore networks in catalyst supports – a percolation theoretical approach to hydrodemetallation, Hung. J. Ind. Chem. 25 (1997) 137–145.
[22] M. Hartmann, Hierarchical zeolites: a proven strategy to combine shape selectivity with efficient mass transport, Angew. Chem. Int. Ed. 43 (2004) 5880–5882.
[23] R. Chal, C. Gérardin, M. Bulut, S. van Donk, Overview and industrial assessment of synthesis strategies towards zeolites with mesopores, Chem. Cat. Chem. 3 (2011) 67–81.
[24] J. García-Martínez, M. Johnson, J. Valla, K. Li, J.Y. Ying, Mesostructured zeolite Y—high hydrothermal stability and superior FCC catalytic performance, Catal. Sci. Technol. 2 (2012) 987–994.
[25] D. Verboekend, N. Nuttens, R. Locus, J. Van Aelst, P. Verolme, J.C. Groen, J. Pérez-Ramírez, B.F. Sels, Synthesis, characterization and catalytic evaluation of hierarchical faujasite zeolites: milestones, challenges and future directions, Chem. Soc. Rev. 45 (2016) 3331–3352.
[26] P.G. Smirniotis, L. Davydov, E. Ruckenstein, Composite zeolite-based catalysts and sorbents, Catal. Rev. Sci. Eng. 41 (1999) 43–119.
[27] T. Titze, C. Chmelik, J. Kullmann, L. Prager, E. Miersemann, R. Gläser, D. Enke, J. Weitkamp, J. Kärger, Microimaging of transient concentration profiles of reactant and product molecules during catalytic conversion in nanoporous materials, Angew. Chem. Int. Ed. 54 (2015) 5060–5064.
[28] F. Hibbe, C. Chmelik, L. Heinke, S. Pramanik, J. Li, D.M. Ruthven, D. Tzoulaki, J. Kärger, The nature of surface barriers on nanoporous solids explored by micro-imaging of transient guest distributions, J. Am. Chem. Soc. 133 (2011) 2804–2807.
[29] J.C. Saint Remi, A. Lauerer, C. Chmelik, I. Vandendael, H. Terryn, G.V. Baron, J.F. M. Denayer, J. Kärger, The role of crystal diversity in understanding mass transfer in nanoporous materials, Nat. Mater. 15 (2016) 401–406.
[30] A.R. Teixeira, C.C. Chang, T. Coogan, R. Kendall, W. Fan, P.J. Dauenhauer, Dominance of surface barriers in molecular transport through silicalite-1, J. Phys. Chem. C 117 (2013) 25545–25555.
[31] A.R. Teixeira, X. Qi, C.C. Chang, W. Fan, W.C. Conner, P.J. Dauenhauer, On asymmetric surface barriers in MFI zeolites revealed by frequency response, J. Phys. Chem. C 118 (2014) 22166–22180.
[32] N.E.R. Zimmermann, S.P. Balaji, F.J. Keil, Surface barriers of hydrocarbon transport triggered by ideal zeolite structures, J. Phys. Chem. C 116 (2012) 3677–3683.
[33] N.E.R. Zimmermann, B. Smit, F.J. Keil, Predicting local transport coefficients at solid-gas interfaces, J. Phys. Chem. C 116 (2012) 18878–18883.
[34] N.E.R. Zimmermann, T. Zabel, F.J. Keil, Transport into nanosheets: diffusion equations put to test, J. Phys. Chem. C 117 (2013) 7384–7390.
[35] S.J. Reitmeier, O.C. Gobin, A. Jentys, J.A. Lercher, Influence of post synthetic surface modification on shape selective transport of aromatic molecules in HZSM5, J. Phys. Chem. C 113 (2009) 15355–15363.
[36] O.C. Gobin, S.J. Reitmeier, A. Jentys, J.A. Lercher, Comparison of the transport of aromatic compounds in small and large MFI particles, J. Phys. Chem. C 113 (2009) 20435–20444.
[37] O.C. Gobin, S.J. Reitmeier, A. Jentys, J.A. Lercher, Role of surface modification on the transport of hexane isomers in ZSM-5, J. Phys. Chem. C 115 (2011) 1171–1179.
[38] N. Hansen, R. Krishna, J.M. van Baten, A.T. Bell, F.J. Keil, Analysis of diffusion limitation in the alkylation of benzene with ethylene over H-ZSM-5 combining quantum chemical calculations, molecular simulations, and a continuum approach, J. Phys. Chem. C 113 (2009) 235–246.
[39] H. Li, M. Ye, Z. Liu, A multi-region model for reaction-diffusion process within a porous catalyst pellet, Chem. Eng. Sci. 147 (2016) 1–12.
[40] A.L. Myers, J.M. Prausnitz, Thermodynamics of mixed gas adsorption, AIChE J. 11 (1965) 121–127.
[41] G.F. Froment, K.B. Bischoff, J. de Wilde, Chemical Reactor Analysis and Design, third ed., Wiley, New York, USA, 2010.
[42] J.W. Evans, M.H. Abbasi, A.J. Sarin, A Monte Carlo simulation of the diffusion of gases in porous solids, Chem. Phys. 72 (1980) 2967–2973.
[43] R.C. Reid, J.M. Prausnitz, B.E. Poling, The Properties of Gases and Liquids, fourth ed., McGraw-Hill, New York, USA, 1987.
[44] G. Wang, E. Johannessen, C.R. Kleijn, S.W. de Leeuw, M.-O. Coppens, Optimizing transport in nanostructured catalysts: a computational study, Chem. Eng. Sci. 62 (2007) 5110–5116.
[45] M.-O. Coppens, G.F. Froment, Fractal aspects in the catalytic reforming of naphtha, Chem. Eng. Sci. 51 (1996) 2283–2292.
[46] O.D. Velev, T.A. Jede, R.F. Lobo, A.M. Lenhoff, Microstructured porous silica obtained via colloidal crystal templates, Chem. Mater. 10 (1998) 3597–3602.
[47] J. Wang, J.C. Groen, M.-O. Coppens, Unified formation mechanism of disordered mesoporous silica, structured by means of nontemplating organic additives, J. Phys. Chem. C 112 (2008) 19336–19345.
[48] S.M. Rao, Rational Design of Hierarchically Structured Catalysts: Multiscale Modeling, Optimization and Experiments Ph.D. thesis, Rensselaer Polytechnic Institute, Troy, NY, USA, 2012.
[49] S.C. Reyes, E. Iglesia, Effective diffusivities in catalyst pellets: new model porous structures and transport simulation techniques, J. Catal. 129 (1991) 457–472.
[50] P. Bai, E. Haldoupis, P.J. Dauenhauer, M. Tsapatsis, J.I. Siepmann, Understanding diffusion in hierarchical zeolites with house-of-cards nanosheets, ACS Nano 10 (2016) 7612–7618.

Please cite this article in press as: S.M. Rao et al., Surface barriers as dominant mechanism to transport limitations in hierarchically structured catalysts – Application to the zeolite-catalyzed alkylation of benzene with ethylene, Chem. Eng. J. (2017), http://dx.doi.org/10.1016/j.cej.2017.04.015